CORE
Metadata, citation and similar papers at core.ac.uk
Provided by Elsevier - Publisher Connector

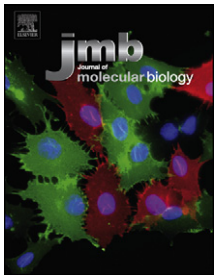

Effects of Bni5 Binding on Septin Filament Organization

Elizabeth A. Booth[1,5,†], **Sarah M. Sterling**[1,†], **Dustin Dovala**[2,6], **Eva Nogales**[1,3,4] **and Jeremy Thorner**[1]

*1 - **Division of Biochemistry,** Biophysics, and Structural Biology, Department of Molecular and Cell Biology, University of California, Berkeley, CA 94720-3202, USA*
*2 - **Program in Microbial Pathogenesis and Host Defense,** Department of Microbiology and Immunology, University of California School of Medicine, San Francisco, CA 94143, USA*
*3 - **Life Science Division,** Lawrence Berkeley National Laboratory, Berkeley, CA 94720, USA*
*4 - **Howard Hughes Medical Institute,** Chevy Chase, MD 20815, USA*

***Correspondence to Jeremy Thorner:** Department of Molecular and Cell Biology, University of California, 526 Barker Hall, Berkeley, CA 94720-3202, USA. jthorner@berkeley.edu*
http://dx.doi.org/10.1016/j.jmb.2016.10.024
Edited by James Sellers

Abstract

Septins are a protein family found in all eukaryotes (except higher plants) that have roles in membrane remodeling and formation of diffusion barriers and as a scaffold to recruit other proteins. In budding yeast, proper execution of cytokinesis and cell division requires the formation of a collar of circumferential filaments at the bud neck. These filaments are assembled from apolar septin hetero-octamers. Currently, little is known about the mechanisms that control the arrangement and dynamics of septin structures. In this study, we utilized both Förster resonance energy transfer and electron microscopy to analyze the biophysical properties of the septin-binding protein Bni5 and how its association with septin filaments affects their organization. We found that the interaction of Bni5 with the terminal subunit (Cdc11) at the junctions between adjacent hetero-octamers in paired filaments is highly cooperative. Both the C-terminal end of Bni5 and the C-terminal extension of Cdc11 make important contributions to their interaction. Moreover, this binding may stabilize the dimerization of Bni5, which, in turn, forms cross-filament braces that significantly narrow, and impose much more uniform spacing on, the gap between paired filaments.
© 2016 The Authors. Published by Elsevier Ltd. This is an open access article under the CC BY-NC-ND license (http://creativecommons.org/licenses/by-nc-nd/4.0/).

Introduction

Septins are a family of GTP-binding and filament-forming proteins found in all eukaryotes (except higher plants) [1,2]. Genes encoding the first representatives of this protein class were originally identified in budding yeast (*Saccharomyces cerevisiae*) in screens for mutants in which cell cycle progression was blocked in a temperature-sensitive (ts) manner [3,4]. Mutations in four cell division cycle (*cdc*) loci isolated in this way (*CDC3*, *CDC10*, *CDC11*, and *CDC12*) each led to specific failure of cytokinesis and the resulting formation of multinucleate cells with multiple, highly elongated buds lacking division septa. Shs1, the fifth septin expressed in mitotically growing cells, was identified by sequence as a septin homolog after the entire *S. cerevisiae* genome was determined [5,6]. The five corresponding gene products localize exclusively at the bud neck during yeast cell division [7,8]. Moreover, the function of each of these proteins is necessary for the formation of a series of uniform striations (approximately 10 nm wide and 28 nm apart) located at the bud neck, first visualized by electron microscopy (EM) [9]. These striations are absent at the restrictive temperature in *cdc3*, *cdc10*, *cdc11*, and *cdc12* mutants but are unaffected in wild-type cells and are aberrant in cells lacking Shs1 [10].

Individual septins [11,12] and multi-septin complexes [13–15] have been heterologously expressed and purified from bacteria. Biochemical and ultrastructural analyses revealed that the mitotic septins assemble into two types of apolar hetero-octameric rods:

0022-2836/© 2016 The Authors. Published by Elsevier Ltd. This is an open access article under the CC BY-NC-ND license (http://creativecommons.org/licenses/by-nc-nd/4.0/).

Cdc11-Cdc12-Cdc3-Cdc10-Cdc10-Cdc3-Cdc12-Cdc11 [14] or Shs1-Cdc12-Cdc3-Cdc10-Cdc10-Cdc3-Cdc12-Shs1 [10], both of which are stable as hetero-octamers in high-salt solution *in vitro*. Under low-salt conditions (<100 mM), Cdc11-capped rods are able to polymerize end to end into long filament pairs [14,16,17], whereas Shs1-capped rods are unable to form end-on-end contacts with themselves but rather associate laterally in a staggered manner to form arcs, spirals, rings, and "bird nests" [10,16]. These assembly processes are promoted on the surface of lipid monolayers that mimic the cytosolic face of the plasma membrane [18,19]. There is evidence from examining mixtures of the two types of rods *in vitro* by EM [10] and by Förster resonance energy transfer (FRET) analysis [16], and genetic evidence *in vivo* [20], indicating that Shs1-capped rods can form heterotypic junctions with Cdc11-capped rods.

Similar to yeast, human septins also form apolar hetero-octameric rods, the most ubiquitiously expressed and abundant of which has the order Sept9-Sept7-Sept6-Sept2-Sept2-Sept6-Sept7-Sept9 [21,22]. Crystal structures for individual human Sept2, Sept3, and Sept7 [23–25] and for a core heterohexamer, Sept7-Sept6-Sept2-Sept2-Sept6-Sept7 [23,26] have been determined. Septins have also been crystallized from other species, such as *Schistosoma masoni* Sept10 [27] and, recently, *S. cerevisiae* Cdc11 [28]. These X-ray structures provide important insight about the GTP-binding pocket in each monomer and how these subunits assemble into a linear rod *via* two distinct, alternating interfaces separated from each other by 180° [23]. On one side, a septin interacts with its neighbor by a so-called G interface because the contacts are made by residues in and around the GTP-binding pocket in each protein. The same septin interacts with its neighbor on the opposite side by a so-called NC interface because the contacts are mediated by residues contributed by structural elements from both the N and C termini of each protein (Fig. 1a). Both structural [26] and biochemical studies [11,29] have delineated the sequence requirements for GTP binding and hydrolysis and the role of nucleotide state on subunit conformation and subunit–subunit interactions. In the work presented here, the terminal subunit Cdc11 is of particular interest. At the NC interface responsible for the homotypic Cdc11–Cdc11 interaction required for the polymerization of hetero-octamers, an N-terminal alpha-helix (α0; residues 6–19) plays a pivotal role [14,16,20]. Furthermore, Cdc11 possesses a pronounced C-terminal extension (CTE; residues 301–415), which contains a C-terminal segment (residues 377–415) with strongly predicted coiled-coil forming propensity and is required for full Cdc11 function [13,30].

The hourglass-shaped collar of septin filaments at the bud neck has three distinct physiological roles: establishing a cortical diffusion barrier [31,32]; promoting membrane curvature either by directly deforming the membrane or indirectly, by recruiting other proteins that do so [33–35]; and serving as a scaffold to recruit other proteins, such as Bni5 [36–38]. During G1, septins accumulate at the incipient bud site and rapidly resolve into a ring, which, at this stage, appears to be a highly dynamic structure based on fluorescence recovery after photobleaching [39,40]. However, during bud emergence, the ring expands into the collar (i.e., during S and early M phase). Then, the septin structures at the bud neck are stable. At mitosis, the collar splits or collapses into two bands (in between which cytokinesis occurs), which, after division, disassemble before the onset of the next cell cycle [38,40,41].

Bni5 was initially identified as a dosage suppressor of the ts growth defect of a *cdc12–6* mutant and was found to also suppress ts alleles in other septin genes [42]. Bni5 localizes to the bud neck after bud emergence during the period when the superstructure in the septin collar is being stabilized [42]. Absence of Bni5 results in growth defects and exacerbates the phenotypes (e.g., elongated cell shape and cell cycle arrest) conferred by septin mutations [30,42]. Reportedly, phosphorylation of Bni5 contributes to its ability to interact with Cdc11 (and Cdc12) and to its dislocation from the bud neck in late mitosis [43], as well as to proper bud morphogenesis [44]. However, subsequent site-directed mutagenesis studies demonstrated that none of the purported sites, alone or in combination, had any effect in two *in vivo* assays for Bni5 function [30]. Most importantly, Bni5 binding to Cdc11 within the septin collar is necessary for efficient recruitment, in turn, of Myo1, the type II myosin required for the assembly of the actomyosin contractile ring that drives plasma membrane ingression for cytokinesis [30,45–47]. However, detailed mechanistic understanding about how Bni5 engages Cdc11 and what effect Bni5 binding has on the supramolecular organization of septin structures was not known. For this reason, we undertook a detailed biophysical analysis of Bni5–septin interaction utilizing both a newly developed FRET-based assay [16,48] and visualization at the ultrastructural level by EM. Our findings provide substantial new insights about the mechanism of Bni5 association with Cdc11 and how it remodels both filament and interfilament organization.

Results

Modeling of septin hetero-octamer and Bni5 structure

Cdc11 is known to be the terminal subunit [14,49] of the yeast septin hetero-octamer (Fig. 1a, top). We generated a model for this hetero-octameric rod by aligning the known structure of Cdc11 (PDB: 5AR1)

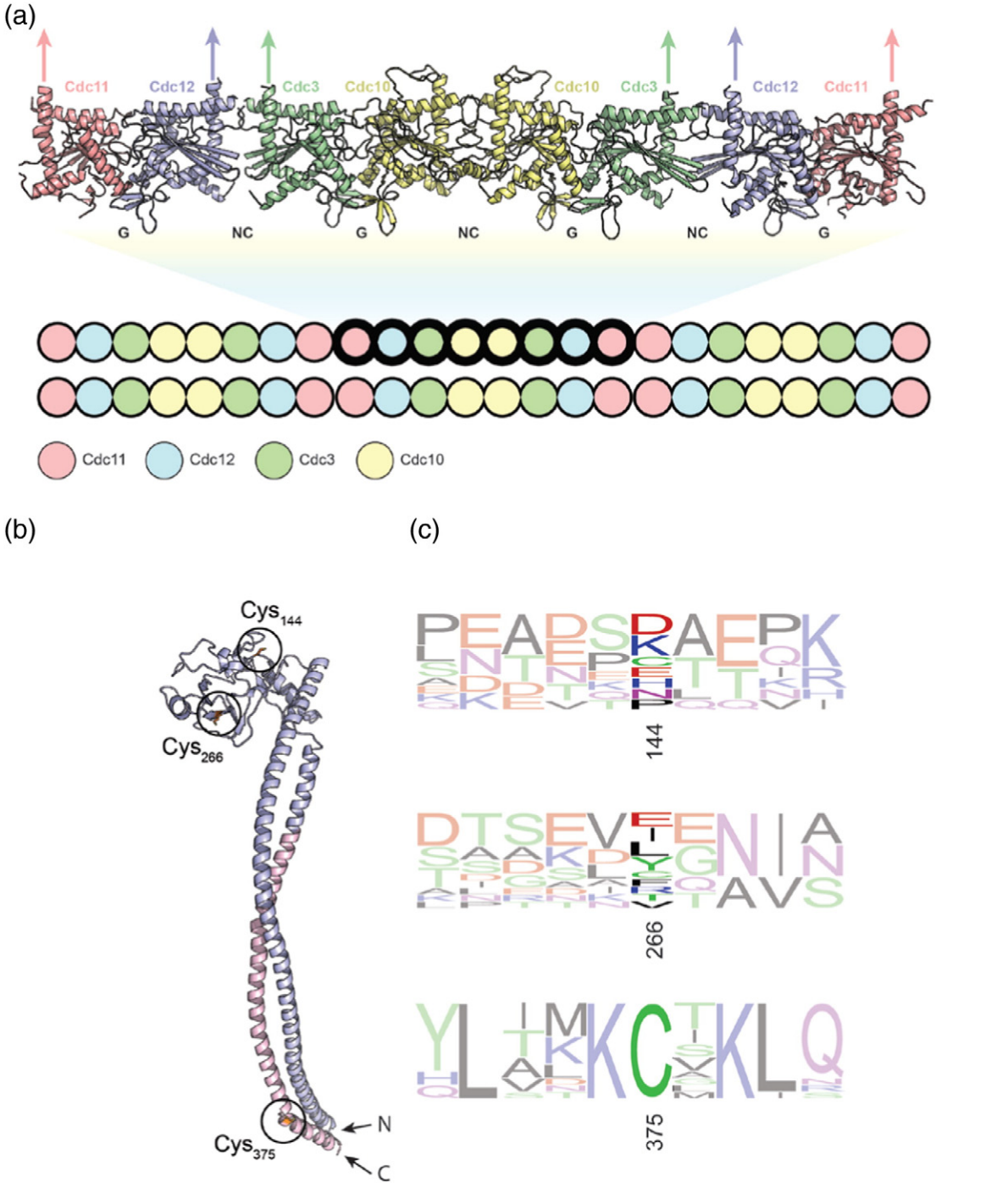

Fig. 1. Structural and sequence features of the yeast septin hetero-octamer and septin-binding protein Bni5. (a) Top: model of the yeast septin hetero-octamer generated in PyMOL by the alignment of the crystal structure of Cdc11 (PDB ID: 5AR1), and Phyre II models of Cdc12, Cdc10, and Cdc3, to the crystal structure of a human septin heterohexamer (PDB ID: 2QAG). Arrows: where CTEs project from α6. Established NC and G interfaces [14] are indicated. Bottom: position of a single hetero-octamer in a paired filament. (b) Left: Bni5 structure predicted by Phyre II. Positions of the three Cys (residues 144, 266, and 375) circled. Pink: segment deleted in a C-terminal truncation mutant examined in this study. (c) Sequence logos [83] anchored on each indicated Cys derived from Clustal Omega alignment [54] of Bni5 homologs from 14 fungal species (height proportional to frequency of residue occurrence).

[28] and the predicted structures for Cdc3, Cdc10, and Cdc12, derived using Phyre II [50], against the known structure of a human septin heterohexamer (PDB: 2QAG) [23]. In every septin crystal structure determined to date, however, the long and flexible CTE has been deleted. Nonetheless, the direction in which each CTE projects out from the corresponding α6 helix in the Cdc11, Cdc12, and Cdc3 subunits is clear and demarcated with an arrow in our model (Fig. 1a, top). Cdc10 lacks a CTE of significant length [13].

We also used Phyre II to align the amino acid sequence of Bni5 against the available crystallographic database to generate a predicted structure, a model in which the N-terminal residues (1–132) and the C-terminal residues (284–448) associate to form an extended coiled- coil connected *via* an internal globular "hinge" domain (residues 133–283; Fig. 1b). This prediction arose from a convincing match (≥95% confidence level) to the similarly arranged alpha-helical coiled-coils and hinge domains of the two large (Structural Maintenance of Chromosomes) subunits of the condensin complex [51,52]. These proteins (Smc2 and Smc4 in *S. cerevisiae*) dimerize in parallel *via* their central hinge domains and have long coiled-coil domains comprising their N- and C-terminal segments, each tipped with the elements of their ATP-binding heads, by which they bind to the smaller subunits of the condensin complex (Brn1, Ycg1, and Ycs4 in yeast) and are thereby linked to a chromosome. Although both the N- and C-terminal ends are clearly the most conserved portions among all Bni5 orthologs, the conservation at the C-terminal end is much more extensive (Fig. S1). Unlike SMC proteins, Bni5 is a gene product restricted to the fungal clade.

Constructs for FRET analysis of septin–septin and septin-binding protein interaction

In low ionic strength solutions *in vitro* (<50–100 mM salt), purified Cdc11-capped hetero-octamers assemble end on end into long paired filaments (Fig. 1a, bottom), which can be readily visualized by EM [14,18]. *In vivo*, the presence of such filaments has been observed by super-resolution microscopy [17]. We recently demonstrated that the formation of the NC interface at each of the Cdc11–Cdc11 junctions during polymerization of individual rods into long filaments can be conveniently measured by FRET [16,48]. In our method, preparations of otherwise purified Cys-less hetero-octamers [53] containing a single introduced Cys residue (E294C) in Cdc11 are labeled with either a donor dye [Alexa Fluor 555 (AF555)] or an acceptor dye [Alexa Fluor 647 (AF647)]. AF555 and AF647 have a reported 50% transfer distance (R_0) of 5.1 nm, and the emission of the donor (AF555) has good spectral overlap with the absorbance of the acceptor (AF647), with only modest tailing into the emission of the acceptor. These properties are very suitable for use in gauging Cdc11–Cdc11 association because the approximate diameter of the G domain of an individual septin is 4 nm [14]. When the two labeled preparations are mixed, and the salt concentration lowered, the formation of Cdc11–Cdc11 junctions between donor dye- and acceptor dye-derivatized rods upon their polymerization yields a marked increase in FRET that is readily monitored in a fluorimeter [16,48]. We also showed that the same approach could be used to follow the interaction of Bni5 (uniformly labeled with acceptor dye at all endogenous Cys residues) with different filament preparations comprising hetero-octamers labeled with a donor dye on a discrete subunit [16]. The highest FRET was observed when the donor dye was located on Cdc11 [16], as expected from other, albeit less direct (mainly genetic), evidence indicating that Bni5 associates with the septin collar *via* interaction with Cdc11 [30,42].

To apply this method to assess the interaction of Bni5 with septins in the most incisive manner possible, we sought to install a single fluorophore at a position most likely to report its most meaningful and physiologically relevant interactions. Fortuitously, native Bni5 possesses only three Cys residues (C144, C266, and C375; Fig. S1). Our model suggests that each should be solvent accessible and, in agreement with that prediction, we showed before that purified Bni5 is labeled with AF647-maleimide to a stoichiometry of 2.7 dye molecules per Bni5 molecule [16]. Phylogenetic comparisons generated using the Clustal Omega algorithm [54] to align *S. cerevisiae* Bni5 against its orthologs from other *Saccharomyces sensu stricto* species (*Saccharomyces arboricola*, *Saccharomyces eubayanus*, and *Saccharomyces kudraivzevii*), and against significantly more divergent fungal species [*Candida glabrata*, *Eremothecium (formerly Ashbya) gossypii*, *Kazachstania (formerly Kloeckera) africana*, *Naumovozyma castellii*, *Naumovozyma dairenensis*, *Tetrapisispora phaffii*, *Torulaspora delbreuckii*, *Vanderwaltozyma polyspora*, *Zygosaccharomyces bailii*, and *Zygosaccharomyces rouxii*] revealed that only Cys375 is invariant and embedded in a sequence that is well conserved (Fig. 1c), including two invariant Lys (374 and 377) residues. In other proteins, nearby Lys residues provide a favorable electrostatic environment that enhances the reactivity of an adjacent Cys with thiol-directed reagents, including maleimides [55]. This segment of Bni5 also contains two invariant Leu (371 and 378) residues, which contribute to the strongly predicted α-helical conformation of this portion of Bni5 [56].

In order to prepare single-dye-labeled derivatives of Bni5 for use in our studies, we used standard site-directed mutagenesis to generate three derivatives of Bni5 that each retained just one of its native Cys residues: Bni5(C266F C375S), Bni5(C144R C375S), and Bni5(C144R C266F), hereafter designated as Bni5 C144, Bni5 C266, and Bni5 C375, respectively. We used our same phylogenetic comparison and other

considerations to inform the indicated replacements made at the other two positions.

FRET analysis of Bni5–septin filament interaction

Upon expression, purification, and labeling of each of these Bni5 derivatives using methods described in detail elsewhere [16,48], we found that the Bni5 C144 and Bni5 C266 mutants exhibited some detectable degradation, as judged by SDS-PAGE visualized by Coomassie dye staining and after labeling with the acceptor dye AF647 (Fig. 2a). In contrast, Bni5 C375 yielded a single intact species, as judged by the same two criteria. Because the only substitution mutation in common between Bni5 C144 and Bni5 C266 is C375S, it is possible that C375 is required for the stability of recombinant Bni5. We cannot rule out, however, that some other substitution at 375 (e.g., Ala) might be better tolerated or, conversely, that different replacements at the other positions (144 and 266) might be less deleterious in combination with C375S. Nonetheless, each preparation contained ample amounts of the corresponding, full-length acceptor dye-labeled protein for use in our FRET studies.

All available evidence both *in vivo* [30,42,43] and *in vitro* [16,42] indicate that Bni5 interacts preferentially with Cdc11. Moreover, in the cell, Bni5 localizes to the bud neck after bud emergence [30,42] during the period when the septin collar becomes stabilized [39,40]. Given that Bni5 associates with the septin collar, which is composed of higher-order filamentous structures assembled from hetero-octamers [9,41,49,57,58], we wanted to examine by FRET the association of acceptor dye-labeled Bni5 C144, Bni5 C266, and

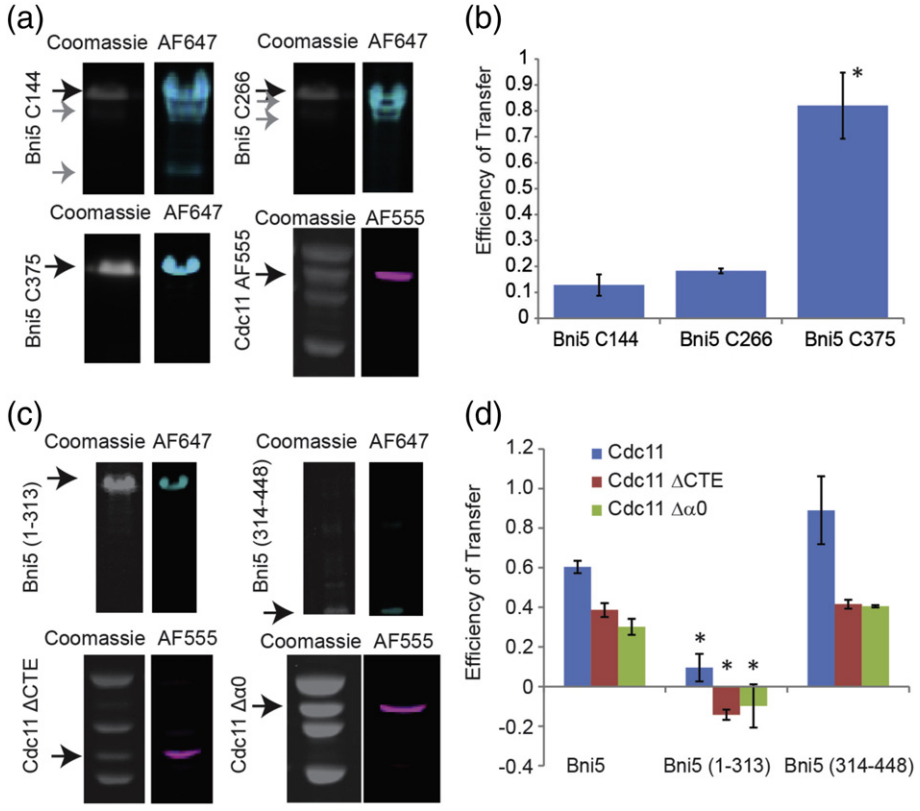

Fig. 2. FRET analysis of Bni5–septin filament interaction. (a) Coomassie and Typhoon scans of Bni5 C144^{AF647} (upper left), Bni5 C266^{AF647} (upper right), Bni5 C375^{AF647} (lower left), and Cdc11^{AF555}-capped septin hetero-octamers (lower right). Black arrows: labeled protein; gray arrows: degradation products. (b) Maximum efficiency of transfer (FRET signal) at an excess concentration of the indicated single-Cys-labeled Bni5^{AF647} protein (500 nM) with filaments composed of Cdc11^{AF555} septin hetero-octamers (25 nM). (c) Coomassie and Typhoon scans of Bni5(1–313) C144^{AF647} (upper left), Bni5(314–448) C375^{AF647} (upper right), Cdc11(ΔCTE)^{AF555} capped hetero-octamers (lower left), and Cdc11(Δα0)^{AF555} capped hetero-octamers. Black arrows: labeled protein. (d) Maximum efficiency of transfer (FRET signal) at an excess concentration of the indicated single-Cys-labeled Bni5^{AF647} protein (500 nM) with filaments composed of the indicated Cdc11^{AF555} septin hetero-octamer (25 nM). Asterisks: for all three types of hetero-octamers [Cdc11-, Cdc11(ΔCTE)-, and Cdc11(Δα0)-capped], the reduction in FRET observed for Bni5(1–313) was statistically significant ($p = <0.05$ by *t*-test) compared to either full-length Bni5 or Bni5(314–448).

Bni5 C375 with otherwise Cys-less hetero-octamers containing Cdc11(E294C) labeled with donor dye under filament-forming conditions.

Thus, to conduct these analyses, and because we previously observed that the formation of filaments is sensitive to the ionic strength (EC_{50} for disruption of Cdc11–Cd11 contacts is 180 mM KCl) [16], we first measured the FRET between Bni5 C375^{AF647} and hetero-octamers capped with Cdc11^{AF555} at varying salt concentrations (Fig. S2). We found, as judged by FRET, that the association between acceptor dye-labeled Bni5 and the donor dye-labeled filaments was salt-sensitive, exhibiting an EC_{50} of 95 mM. This effect represents an influence of ionic strength on Bni5–Cdc11 binding because this salt concentration is not sufficient to disrupt the filaments themselves. Based on these observations, we therefore conducted all subsequent FRET analyses of Bni5–septin interaction at 45 mM KCl.

Having established these optimum conditions, we then compared the interaction between Bni5 C144, Bni5 C266, or Bni5 C375, each labeled with acceptor dye at the indicated Cys, and filaments labeled with the donor dye on Cdc11(E294C). We found that Bni5 C375^{AF647} reproducibly displayed a FRET efficiency that was at least fourfold higher than either Bni5 C144^{AF647} or Bni5 C266^{AF647} (Fig. 2b), even though control experiments confirmed by both a co-sedimentation assay and direct visualization by EM that each of these dye-labeled Bni5 variants binds to septin filaments with equivalent efficacy (Fig. S3). These results clearly indicate, first, that the C-terminal portion of Bni5 is in more intimate contact with Cdc11 than the regions occupied by C144 and C266. Second, the fact that the FRET exhibited with Bni5 C144^{AF647} and Bni5 C266^{AF647} were much lower and quite comparable to each other is consistent with our predicted Smc-like structure for Bni5, where the C144 and C266 are located in a globular domain situated at the opposite end of a highly elongated rod-like coiled-coil that is far from C375 (Fig. 1b).

Under the same conditions, we could not detect the interaction of Bni5 C375^{AF647} with septin structures assembled from hetero-octamers capped with Shs1(C29V C148S) E344C^{AF555} (Fig. S4; for further information, see Supplementary Results).

Structural elements contributing to Bni5–Cdc11 association

To confirm that it is the C-terminal portion of Bni5 that associates with Cdc11, we generated two constructs that produced, respectively, an N-terminal fragment, Bni5(1-313; C266F) C144, and a smaller C-terminal fragment, Bni5(314-448) C375. These two Bni5 derivatives were produced, purified, and labeled with acceptor dye, in the same way as for the full-length Bni5 (Fig. 2c, upper panels). To assess which aspects of Cdc11 in filaments assembled from Cdc11-capped hetero-octamers are required for the high-affinity binding of Bni5, we also prepared hetero-octamers capped with two Cdc11 mutants, Cdc11(Δ357–415) E294C, which lacks its CTE but is still able to assemble into hetero-octamers and polymerize into long paired filaments in solution, and Cdc11(Δα0) E294C, which is still able to assemble into hetero-octamers but displays a markedly reduced ability to polymerize into long paired filaments in solution [14]. Hetero-octamers containing these Cdc11 variants were produced, purified, and labeled with donor dye, in the same way as for hetero-octamers containing wild-type Cdc11 (Fig. 2c, lower panels).

As judged by the observed FRET, we found, first, that the C-terminal fragment of Bni5 was able to interact with filaments composed of Cdc11-capped hetero-octamers just as robustly as full-length Bni5 (Fig. 2d and Fig. S5), whereas the N-terminal fragment of Bni5 did not exhibit any detectable FRET above the background (Fig. 2d and Fig. S5). These findings explain why, in our initial observations, Bni5 C375 exhibited much stronger FRET with Cdc11 than either Bni5 C144 or Bni5 C266. These results also are consistent with genetic observations that showed that C-terminal truncations that remove as few as 25 residues cause a loss of Bni5 function *in vivo*, whereas even much larger N-terminal truncations do not [30]. Second, we found that the removal of the CTE of Cdc11 caused a pronounced reduction in the FRET observed with both full-length Bni5 and the C-terminal fragment of Bni5, but it did not abrogate the interaction completely (Fig. 2d). In titration experiments, wherein the concentration of Bni5 added to reach the half-maximal of the observable FRET signal (EC_{50}) provides only a very rough proxy for K_d (because none of the curves reached saturation), we found that the removal of the CTE of Cdc11 substantially weakened its affinity for the C-terminal fragment of Bni5 (Fig. S5). Specifically, Bni5(314–448)^{AF647} interaction with filaments composed of hetero-octamers capped with otherwise wild-type Cdc11 E294C^{AF555} exhibited an apparent EC_{50} of 734 nM, whereas Bni5(314–448)^{AF647} interaction with filaments composed of hetero-octamers capped with Cdc11(ΔCTE) E294C^{AF555} exhibited an apparent EC_{50} of 2.1 μM. Moreover, Bni5(314–448)^{AF647} interacted with filaments composed of hetero-octamers capped with Cdc11(Δα0) E294C^{AF555} with an apparent EC_{50} of 614 nM, consistent with the fact that the CTE is still present. Likewise, septin hetero-octamers capped with Cdc11(Δα0) immobilized on beads were clearly able to retain full-length Bni5 (Fig. S6), confirming that residues in the Δα0 segment of Cdc11 are not required for the recruitment of Bni5 to septin hetero-octamers. Third, if our model predicting a coiled-coil interaction between its N- and C-terminal ends (Fig. 1b) is indeed a reasonable approximation of the structure of Bni5, our FRET results with the two Bni5 fragments indicate that the helical C-terminal portion of Bni5 interacts directly

with Cdc11 in septin filaments, specifically making significant contact with the Cdc11 CTE.

As an independent means to assess Bni5–septin interaction at a more macroscopic level, we used fluorescence microscopy to examine the efficiency of association of dye-labeled Bni5 with dye-labeled septin filament networks. We found, first, that full-length Bni5 reliably displayed complete co-localization with filaments generated with Cdc11-capped hetero-octamers and similarly with the structures generated from Cdc11(Δα0)-capped hetero-octamers, which do not polymerize into filaments but rather form aggregates [16], but, in many images, displayed much less tendency to co-localize with filaments generated with Cdc11(△CTE)-capped hetero-octamers (Fig. S7). Second, the N-terminal fragment, Bni5(1–313), exhibited no detectable co-localization with the assemblies generated even with Cdc11-capped hetero-octamers, whereas the C-terminal fragment Bni5(314–448) exhibited extensive co-localization with Cdc11-capped hetero-octamers and some apparent ability to associate with both Cdc11(Δα0)-capped and Cdc11(△CTE) hetero-octamers (Fig. S8).

Properties of Bni5 interaction with Cdc11-containing septin filaments

To measure the affinity of full-length Bni5 C375^{AF647} binding to septin filaments assembled from Cdc11^{AF555}-capped hetero-octamers, titration experiments were conducted. Principal component analysis of the resulting FRET spectra (see Fig. S2) revealed just a single principal component accounting for > 98% of the variance in the system, indicating that the observed FRET arises from single bimolecular interactions between a Cdc11^{AF555} donor and a Bni5 C375^{AF647} acceptor. Replotting of the principal component coefficients at each concentration tested yields a binding curve (Fig. 3a). Titrations conducted at two different concentrations (25 and 50 nM) of donor dye-labeled filaments yielded very similar values for the apparent K_d of the binding of acceptor dye-labeled Bni5 (194 and 218 nM, respectively). This value (average 206 nM) is in good agreement with K_d values for this interaction derived previously by this method [16] and another technique [15]. Strikingly, the titration curves obtained were clearly sigmoidal (Fig. 3a), indicating cooperativity in Bni5 recruitment to the septin filaments. Indeed, curve fitting yielded calculated Hill (n) coefficients in the range of 1.4–1.8. We did not observe this cooperative behavior in the binding of Bni5 to septin filaments previously; in our prior study, however, Bni5 was labeled with dye at all three of its native Cys [16], possibly masking this behavior or introducing dye at a position that interfered with this behavior.

Revealingly, when these same titration experiments were repeated with Bni5 C375^{AF647} and septin assemblies generated from hetero-octamers capped with Cdc11(Δα0)^{AF555}, both the binding affinity (154 nM) and degree of cooperativity (n = 2.1) were similar to the values obtained with hetero-octamers capped with wild-type Cdc11^{AF555}, whereas cooperativity was eliminated (n = 0.92) with hetero-octamers capped with Cdc11(△CTE)^{AF555}, as reflected in the hyperbolic curve observed (Fig. 3b). These observations again indicate that it is the CTE of Cdc11 that makes a significant contribution to the cooperative binding of Bni5. In this regard, however, unlike the C-terminal fragment of Bni5, Bni5(314–448)^{AF647}, whose affinity for filaments generated from Cdc11-capped hetero-octamers was greatly diminished by the removal of the Cdc11 CTE, the affinity of full-length Bni5 for filaments generated from hetero-octamers capped with Cdc11(△CTE)^{AF555} (apparent K_d = 135 nM) was close to that observed for filaments assembled from hetero-octamers capped with wild-type Cdc11 (i.e., likely within the experimental error of our system). Collectively, and in light of our model for Bni5 structure (Fig. 1b), these findings suggest that residues in the C-terminal α-helical segment of Bni5 make primary contact with the CTE of Cdc11 and, perhaps, that residues within the N-terminal α-helical segment of Bni5 make primary contact with the globular GTP-binding domain of Cdc11 or, more likely, with the N-terminal α-helical segment of a Bni5 bound to either the opposite or adjoining Cdc11, contributing to dimerization (see next section). However, aside from stabilizing the C-terminal segment, the N-terminal segment can only make a very minor contribution to Bni5–Cdc11 association because, as we have shown here using a C-terminal fragment of Bni5 (Fig. 2) and using the analysis of N-terminal truncations *in vivo* [30], the removal of as many as 300 or more N-terminal residues has a minimal effect on Bni5 binding to Cdc11 *in vitro* and to Bni5 function in the cell.

Oligomerization properties of Bni5

There are many potential sources of cooperativity in the interaction of Bni5 with the terminal subunit–subunit junctions present in the paired filaments assembled from Cdc11-capped hetero-octamers. The fact that the removal of the CTE from Cdc11 eliminated the cooperative binding of Bni5 indicates that it makes a major contribution to the observed behavior. One possible explanation for this effect is that Bni5 has some propensity to self-associate, and this tendency is enhanced when Bni5 associates with the CTE of Cdc11. To assess whether Bni5 has any intrinsic capacity to oligomerize, we examined its hydrodynamic properties in solution using, first, analytical ultracentrifugation [59]. Native Bni5 has a molecular mass of 49.7 kDa; for its purification, however, we used a $(His)_8$-3C protease cleavage site-Bni5 fusion (52.8 kDa) and examined its sedimentation behavior directly (i.e., without removing the

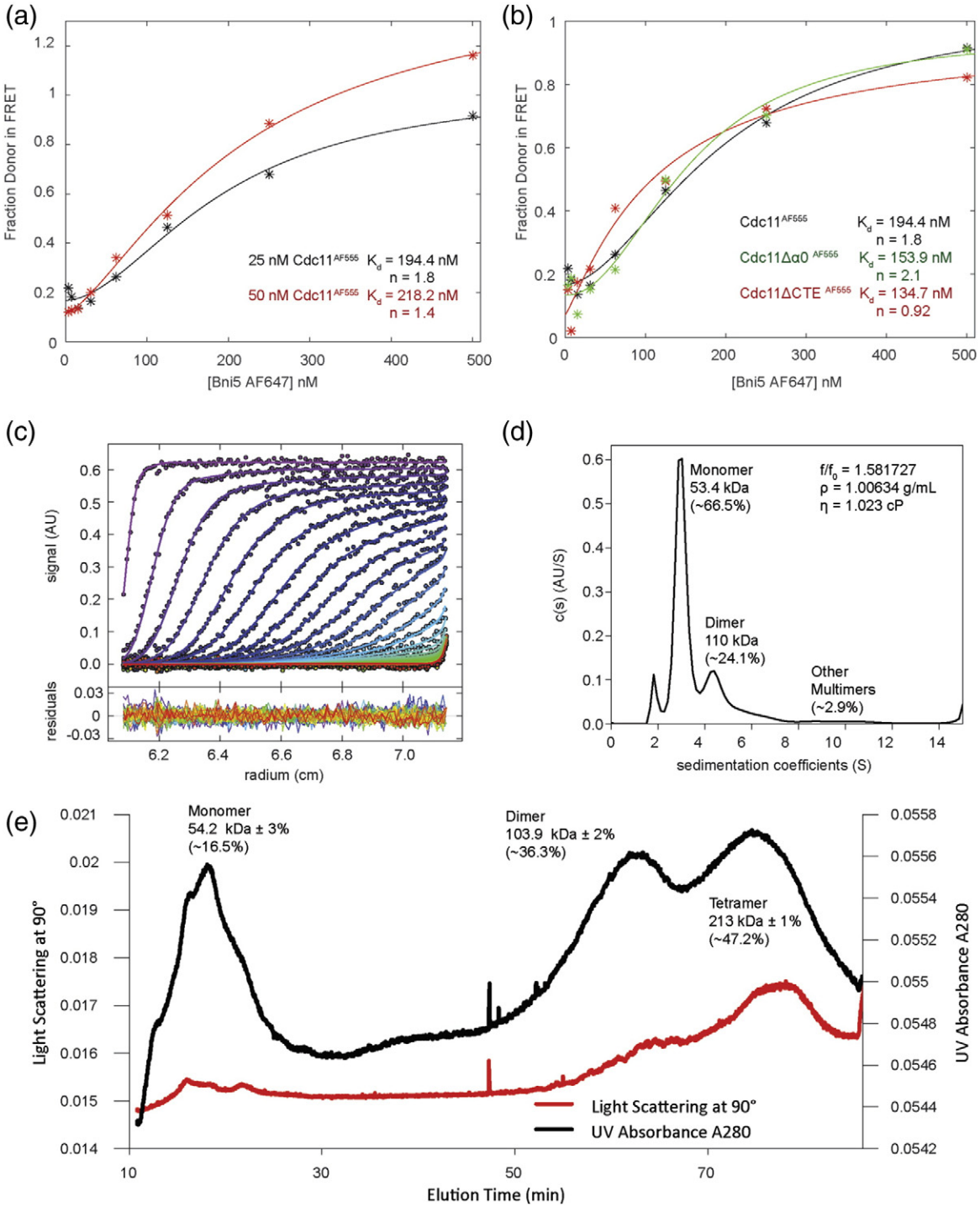

Fig. 3. Bni5 binds cooperatively to filaments of Cdc11-capped hetero-octamers and exhibits a monomer–dimer–tetramer transition. (a) Titration of two fixed concentrations of septin filaments containing $Cdc11^{AF555}$ (black: 25 nM; red: 50 nM) with the indicated increasing concentrations of Bni5 $C375^{AF647}$ (from 8 to 500 nM). (b) Titration curves of a fixed concentration (25 nM) of the septin structures assembled from hetero-octamers capped with $Cdc11^{AF555}$ (black), $Cdc11(\Delta\alpha0)^{AF555}$ (green), or $Cdc11(\Delta CTE)^{AF555}$ (red) with increasing concentrations of Bni5 $C375^{AF647}$, as in (a). (c) Analytical ultracentrifugation of purified Bni5. Top: raw scans of the protein distribution (absorbance) across the flow cell during the time course of sedimentation; bottom: the associated residuals. (d) Plot of the calculated sedimentation coefficients for the species detected in (c) with their corresponding molecular masses shown and an estimated frictional coefficient (f/f_0) derived from the same analysis. The approximate percentage of each species is calculated and displayed. (e) A preparation of free Bni5 was subjected to FFF-MALS, as described in Materials and Methods.

purification tag; Fig. 3c). The same Bni5 derivative was used for the majority of the other analyses presented in this study. Prior work has demonstrated that Bni5 function tolerates fluorescent protein- and epitope-tags attached to its N terminus, but it is much less tolerant of the same or similar tags attached to its C terminus [30]. Based on the sedimentation rates observed, we detected two species of calculated apparent molecular masses of 53.4 (major peak) and 110 kDa (minor peak; Fig. 3d), in excellent agreement with the values expected for a monomer and dimer of Bni5. From these same data, an apparent frictional coefficient can also be calculated, which was 1.58, indicative of a highly elongated molecule and consistent with our predicted structure of Bni5. Therefore, as one possible explanation for the observed cooperativity in Bni5–Cdc11 interaction, Bni5 association with Cdc11 might promote a shift in the Bni5 monomer–dimer equilibrium in favor of the dimer.

To confirm the propensity of Bni5 to self-associate, we used an orthogonal analysis technique. For this purpose, we chose field-flow fractionation (FFF) [60,61] analyzed by multi-angle light scattering (MALS; FFF-MALS). Given the evidence we already obtained from analytical ultracentrifugation for some degree of Bni5 oligomerization, we generated several constructs to assess the contributions that portions of Bni5 may make to its capacity for self-association. Toward this end, we examined full-length Bni5, Bni5(1–313), MBP-Bni5(314–448), and Bni5(ΔHD) (in which residues 133–283, representing the predicted hinge domain, have been deleted and replaced with an Ala_{10} linker). Bni5 exhibited three distinct monodisperse populations with molecular weights corresponding to monomeric, dimeric, and tetrameric forms (Fig. 3e; Table S1). We observed the same monomer, dimer, and tetramer distribution for Bni5(1–313) (Fig. S9a; Table S1), whereas the Bni5(ΔHD) and MBP-Bni5(314–448) constructs displayed only a single monomeric species (Fig. S9b and c; Table S1). These findings suggest, first, that the hinge domain of Bni5 (residues 133–283) is involved in its ability to multimerize, as in SMC proteins. Second, these findings indicate that the C-terminal portion of Bni5 does not have an independent capacity to mediate any self-association, consistent with our evidence that it has a specific role in interacting with Cdc11 and especially with the CTE of Cdc11.

Visualization of Bni5 binding to septin filaments by EM

As another means to interrogate how Bni5 binds to septin filaments assembled from Cdc11-capped hetero-octamers under our conditions (45 mM KCl), and the consequences of that binding, we used EM analysis. While our work was in progress, an EM examination was reported by others [47] showing that the presence of Bni5 produced apparent cross-bridging at regular intervals between septin filament pairs. To gain more in-depth mechanistic insight, we conducted a comparative study of the supramolecular organization of septin filaments in the absence and presence of Bni5, first, to verify that Bni5 is recruited exclusively to the Cdc11–Cdc11 junctions in polymerized filaments and, second, to explore the change(s), if any, that septin filaments undergo upon Bni5 binding.

We noted that prolonged incubation with Bni5 can cause the packing of filaments into bundles and larger aggregates (Figs. S7 and S8). Hence, in our EM analysis, the stoichiometry between Bni5 and Cdc11-capped hetero-octamers was kept low (≤5-fold) and the times of incubation were kept short (<5 min). Visual inspection of the raw images of septin filaments generated from the Cdc11-capped hetero-octamers showed the expected long paired filaments observed previously by us [14] and others [47] and confirmed that, under our conditions, in the Bni5-containing samples, many of the filament pairs were occupied by Bni5, but far from all, as expected (Fig. S10a). Two major differences were observed when comparing the absence and presence of Bni5 (Fig. S10a and b). First, in the absence of Bni5, the gap between the two filaments in any given pair is quite variable over its length (Fig. S10c, d, and e), whereas in the presence of Bni5, the spacing between the two filaments in a pair is narrower and much more uniform (Fig. 4 and Fig. S10a). Second, in the absence of Bni5, there was no observable density between the filament pairs (Fig. S10b and d), whereas when Bni5 was present in those filament pairs that were decorated, there was a prominent and periodic density between the paired filaments (Fig. 4 and Fig. S10a).

To further assess the characteristics of the filaments with Bni5 bound, we generated at least 250 2D class averages of such paired filaments (Fig. 4a and Fig. S3). Visual inspection of these images established, first, that when Bni5 is present, the profile of the interfilament region comprises a doublet of densities, sandwiched on each side by a pair of septin subunits (Fig. 4a, upper left, and Fig. S3). Second, the number of septin subunits from one density to the next is eight (Fig. 4a, upper center, and Fig. S3). Third, histograms of the distance between filaments determined from the radon transforms of corresponding 2D class averages (Fig. S10e), which were normalized and fit to appropriate probability density functions (see Materials and Methods), gave a mean interfilament distance of 19.6 nm (σ = 5.2 nm) in the absence of Bni5, whereas for filament pairs clearly decorated with Bni5, the distance was contracted to 9.3 nm (σ = 3.24 nm; Fig. 4b). Under our conditions, not all paired filaments were decorated with Bni5 (Fig. S10a), and thus, as expected, a minority of the 2D class averages obtained in the presence of Bni5 (~29%, based on the mixture weight) displayed an interfilament spacing of 18.0 nm (σ = 3.8 nm), very similar to that seen in the absence of Bni5 (Fig. 4b).

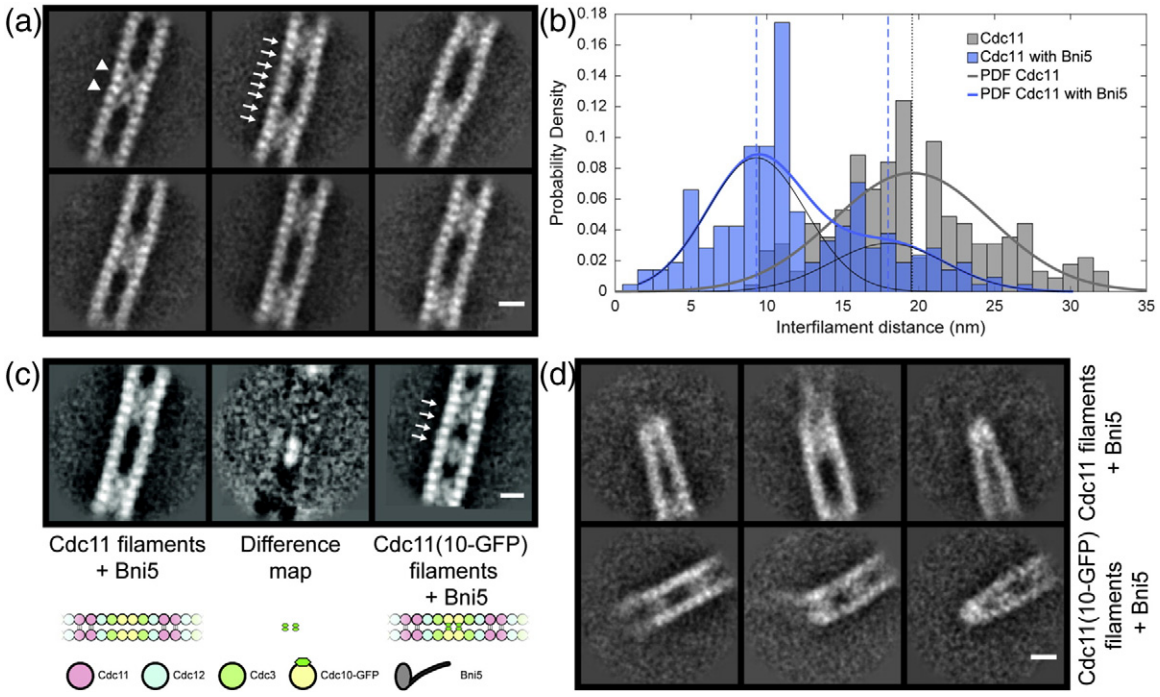

Fig. 4. Bni5 binds at Cdc11–Cdc11 junctions and reorganizes paired septin filaments. (a) Representative 2D class averages of paired septin filaments generated from Cdc11-capped hetero-octamers (50 nM) in the presence of Bni5 (250 nM). White triangles: density between the filaments; white arrows: number of septin subunits between densities. (b) Histogram of the size of the gap (interfilament distance) between filament pairs in the absence (gray) and presence (blue) of Bni5, each fit to a normal distribution. Probability density functions were fit to each data set. Dotted gray line: mean of the distribution in the absence of Bni5; dashed blue lines: means of the two normal distributions in the presence of Bni5. (c) Aligned difference maps comparing a single 2D class average of paired filaments with Bni5 (*left*) to a single 2D class average of paired filaments in the absence of Bni5 (center) and to a single 2D class average of paired containing Cdc10-GFP (right). White arrows: number of septin subunits between the GFP and Bni5 densities. (d) Representative 2D class averages of filament ends. Top: filaments with Bni5; Cdc10-GFP-containing filaments with Bni5. Scale bars represent 10 nm.

EM analysis of Bni5 binding to the Cdc11 subunits in septin filaments

In a septin filament, there are only two types of subunits that are situated with an eight-subunit periodicity: the terminal Cdc11 subunits at each end of the hetero-octameric rod, and the pair of Cdc10 subunits at the center of every hetero-octamer (Fig. 1a, lower). We used two independent approaches to further confirm that Bni5 binds exclusively to the Cdc11 subunits in polymerized hetero-octamers. First, filament preparations generated from purified Cdc11-capped hetero-octamers that also contained Cdc10-GFP as the sole source of this subunit to provide an internal fiducial mark, as we have described before [14], were decorated with Bni5. Compared to filaments containing native Cdc10 decorated with Bni5, these filaments displayed an additional periodic density every four subunits (Fig. 4c, right), which we could clearly attribute to the presence of Cdc10-GFP on the basis of a difference map (Fig. 4c, center) and its location (Fig. S11a). Cdc11 lies four subunits away from Cdc10 (Fig. 1a, lower); hence, the density attributable to Bni5 is associated only with Cdc11. As observed for filaments composed of Cdc11-capped hetero-octamers, the interfilament spacing of the filaments composed of Cdc11-capped hetero-octamers containing Cdc10-GFP was contracted from 19.1 nm (σ = 4.2 nm) in the absence of Bni5 down to 9.1 nm (σ = 2.92 nm) in the presence of Bni5 (Fig. S11b), although again, there was a minority population (~42%, based on the mixture weight) with a spacing of 17.2 nm (σ = 4.50 nm) similar to the undecorated filaments.

The second approach we used to corroborate that the Bni5 density is intimately juxtaposed to Cdc11 was taken advantage of the fact that at the very tip of a filament, the free end is terminated by a Cdc11 subunit [14]. Hence, in the presence of Bni5, such ends should be decorated with density, as we, in fact, observed in representative 2D class averages (Fig. 4d, upper panels). Moreover, at the ends of filaments generated from Cdc11-capped hetero-octamers containing Cdc10-GFP, there should be

an additional density situated four subunits away from the density attributable to Bni5 at the end, as we also observed was the case (Fig. 4d, lower panels), even though these representative 2D class averages were not as well resolved as those derived from aligning internal segments of filaments because free filament ends are much less abundant. In summary, and in agreement with our FRET analysis and all of the other evidence available, the density attributable to Bni5 is specifically associated with the Cdc11–Cdc11 junctions in septin filaments.

EM analysis of the role of the Cdc11 CTE in Bni5 recruitment

To further assess the contribution of the CTE of Cdc11 in the binding of Bni5 to septin filaments, we examined the ultrastructure of septin filaments assembled from purified hetero-octamers capped with Cdc11(ΔCTE) in the absence and presence of Bni5. We found by visual inspection that even in the presence of Bni5, the majority (~73%, based on the mixture weight) of the representative 2D class averages of filament pairs (Fig. 5a, top) did not display any reproducible density between them and exhibited an interfilament spacing [15.2 nm (σ =4.2)] similar to that of filaments assembled from Cdc11(ΔCTE)-capped hetero-octamers in the absence of Bni5 [16.9 nm (σ = 4.7 nm)], which, in both cases, are a bit narrower than for filaments assembled from hetero-octamers capped with wild-type Cdc11 in the absence of Bni5 (~19 nm; Fig. 4). These observations suggest, first, that the CTEs on the four Cdc11 subunits at the Cdc11–Cdc11 junctions in paired filaments may contribute to setting the distance of the interfilament gap. Second, in the absence of the Cdc11 CTE, Bni5 is not able to decorate the majority of the paired filaments under our conditions. In rare instances, some density appeared between the filaments (Fig. 5a, top left), but it was very poorly resolved, indicative of a lack of fixed organization. Indeed, if any Bni5 is bound, it cannot be associated with the Cdc11 subunits in any fixed position or orientation, in marked contrast to what we observed with filaments containing wild-type Cdc11 (Fig. 4).

In these 2D class averages, we also observed a minor population of filament pairs derived from Cdc11(ΔCTE)-capped hetero-octamers that appeared to be overlaid or twisted upon one another (Fig. 5a, bottom). These profiles seemed to occur more frequently in the presence of Bni5 than in its absence. In these cases, the apparent interfilament spacing was reduced to 5.3 nm (σ = 2.07 nm). This behavior may reflect the influence of some degree of binding of Bni5 to these filaments, even though all of the Cdc11 subunits lack their CTE, in agreement with the interaction seen between Bni5 and Cdc11(ΔCTE)-containing filaments in our FRET analysis (Fig. 2d). Nonetheless, the ability of filaments lacking the CTE of Cdc11 to clearly retain and fix the position of Bni5 was markedly less efficient than for filaments containing wild-type Cdc11.

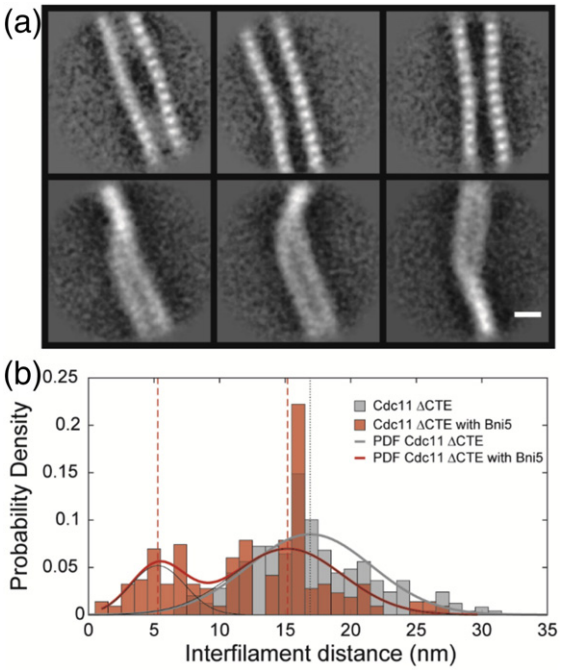

Fig. 5. The CTE of Cdc11 is required for efficient Bni5 recruitment. (a) Representative 2D class averages of paired filaments assembled with hetero-octamers capped with Cdc11(ΔCTE) (50 nM) and Bni5 (250 nM). Scale bar represents 10 nm. (b) As in Fig. 4b, normalized histograms of the interfilament distance of paired filaments assembled from Cdc11(ΔCTE)-capped hetero-octamers in the absence (gray) and presence (orange) of Bni5 probability density functions were fit to each data set. Dotted gray line: mean of the normal distribution in the absence of Bni5; dashed orange lines: means of the mixture of two normal distributions in the presence of Bni5.

Discussion

In the work describing the initial discovery of Bni5 [42], it was reported on the basis of the two-hybrid method, *in vitro* binding (glutathione *S*-transferase pull-downs), and protein-localization studies that Bni5 interacts exclusively with the G domain of Cdc11 and, moreover, that a Cdc11 mutant lacking its CTE, namely Cdc11(Δ347–415), did not display any obvious growth or morphology phenotype, unlike *bni5Δ* cells, which displayed defects in cytokinesis. In marked contrast, in subsequent work, it was demonstrated by two other groups that cells expressing an even less severe truncation, Cdc11(Δ372–415), as the only source of this septin, displayed severe cytokinesis defects and elongated buds [13,62]. Those studies and subsequent work have amply confirmed that the CTE of Cdc11 does not seem to play a major role in

septin filament assembly, but it is rather required for proper septin collar function [13,20,30].

Indeed, the studies we report here amply confirm, first, that the interaction of Bni5 with septin filaments composed of Cdc11-capped hetero-octamers is mediated exclusively through its direct physical association with the Cdc11 subunits. Second, we have demonstrated here that the CTE of Cdc11 plays a major role in establishing the contacts necessary for the stable recruitment of Bni5 to assembled septin filaments. Third, in agreement with prior inferences based on genetic findings [30], we also demonstrated that the C-terminal sequence of Bni5 is critical for its binding to septin filaments. Fourth, our studies revealed the novel insight that Bni5–Cdc11 association creates a periodically cross-braced structure in which the paired septin filaments are drawn close together (<10 nm) and in which there is much more uniform spacing between the filament pairs. Once formed, these collective protein–protein interactions would be expected to stabilize and rigidify this reorganized form of the paired filaments.

Our modeling of Bni5 structure shows that it has remarkable similarity to the hinge and coiled-coil segments of SMC proteins. Moreover, like SMC proteins, using analytical ultracentrifugation, we found that Bni5 has a propensity to dimerize and is a highly elongated molecule, also consistent with our model. Additionally, we observed that the CTE of Cdc11 is critically important for the cooperative binding of Bni5 to septin filaments. Based on these considerations, the most conservative model (Fig. 6) to explain our FRET analysis of the mode of Bni5–septin binding, our EM images, and the cooperativity of Bni5 binding is as follows. First, the antiparallel coiled-coil of a Bni5 monomer is captured by forming a three-helix bundle with the CTE of a Cdc11 subunit [63], in which the C-terminal helix of Bni5 makes the primary contacts with the Cdc11 CTE. This tethering raises the effective local concentration of Bni5 (and leaves its hinge domain freely available). Our evidence indicates that Bni5 dimerizes *via* a hinge domain–hinge domain interaction, as do the SMC proteins, presumably in parallel fashion. If so, once a single Bni5 molecule is bound, the capture of the next Bni5 monomer can now occur *via* two additive contacts—its coiled-coil forming a three-helix bundle with the CTE of a nearby Cdc11 subunit and its hinge domain dimerizing with the hinge domain of the adjacent already-tethered Bni5 monomer. It is also possible that further enhancement in Bni5 binding at every Cdc11–Cdc11 junction could arise from the pairing of bound Bni5 dimers to form a homotetramer. Furthermore, as more Bni5 molecules bind, more of the lengths of the paired filaments draw closer together, making it easier for more adjacently bound Bni5 monomers to dimerize (and tetramerize)—a "zippering up" effect. Collectively, these features readily explain the observed cooperativity in Bni5 binding to Cdc11-containing filaments. Moreover, we also obtained some evidence that, to a degree, the interfilament spacing is constrained in the absence of Bni5 by the CTEs of the Cdc11 subunits. Hence, by sequestering the CTEs of the Cdc11 subunits, Bni5 binding would alleviate this distance constraint, allowing the pair of filaments to draw much closer together, as we observed.

These properties of Bni5–septin filament interaction likely explain why the presence of Bni5 is important for the reorganization and stabilization of the septin collar prior to M phase of the *cdc*. Moreover, it is clear that Bni5 binding generates a platform onto which Myo1, the type II myosin necessary for contractile ring assembly, is bound [30,45]. However, in addition, Bni5 binding may hold septin filaments in such a manner that permits the sequential recruitment of other classes of septin-binding proteins that are able to span the ~9-nm spacing between filaments but would otherwise be unable to span the ~19-nm gap when Bni5 is absent. Conversely, by driving a narrowing of the gap between filaments, the binding of Bni5 may have a role in "squeezing out" or ejecting septin-associated binding proteins that bind inside the gap between filaments, such as the Cdc42-GTP effector Gic1, which associates with filaments by binding to the Cdc10 subunits [64] and is thought to participate in the initial recruitment of septin complexes to the plasma membrane [65].

This study has provided new mechanistic insights about the septin–Bni5 interaction, illustrating how recruitment to a specific septin subunit and, hence, to a specific subcellular location is achieved. Given the role of the Cdc11 CTE in this process, and because all septin crystal structures currently lack any information about their respective CTEs, it may be possible to crystallize a complex between Bni5 and a CTE-containing fragment of Cdc11 to gain further molecular-level detail about how the exquisite specificity in this interaction is attained.

Materials and Methods

Expression, purification, and labeling of septin complexes and Bni5 for FRET analysis

Septin subunits were co-expressed in two DUET™ vectors (EMD Millipore) with compatible origins of replication essentially as described previously [16,48], using otherwise Cys-less septins Cdc3(C124V C253V C279V), Cdc10(C266S), Cdc11(C43F C137A C138A), 6xHis-Cdc12(C40A C278S), and Shs1(C29V C148S), wherein a single Cys was reinstalled at a chosen location in a given subunit by site-directed mutagenesis [66], which, as we have shown previously, are able to support yeast cell viability and form hetero-octameric complexes *in vitro* indistinguishable from wild-type septins [53]. Using sequence- and ligation-independent

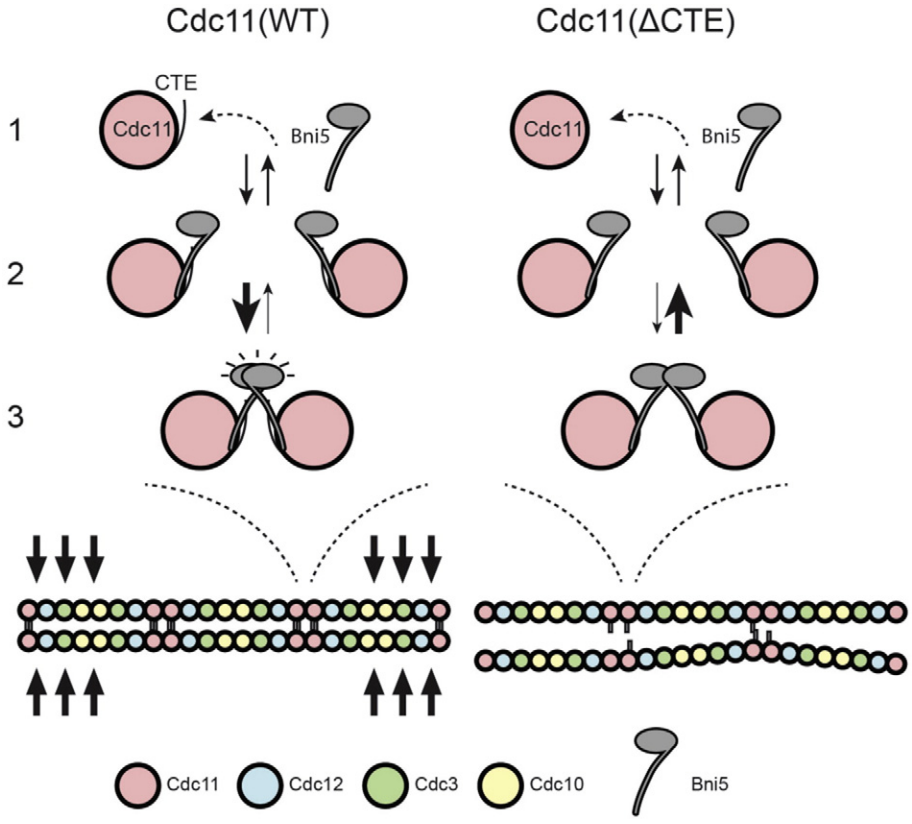

Fig. 6. Schematic summary of the properties of Bni5 binding to septin filaments. The CTEs of Cdc11 impose a constraint that keeps paired filaments apart. One Bni5 monomer binds to one Cdc11 subunit, mediated largely by the interaction of residues in the C-terminal portion of the coiled-coil of Bni5 with the CTE of Cdc11. Tethering of one Bni5 monomer promotes the cooperative recruitment of and dimerization with the next incoming Bni5 molecule. By sequestering the CTEs of Cdc11, the filaments are able to draw closer together and take on a very uniform interfilament spacing. As more Bni5 molecules bind, more of the filaments draw closer together, making it easier for more adjacently bound Bni5 monomers to dimerize. When the Cdc11 CTE is absent, Bni5 recruitment is inefficient, cooperativity of Bni5 binding is lost, and paired septin filaments are more disorganized.

cloning [67] and site-directed mutagenesis, CTE-less truncations of Cdc11 and Shs1 were also generated.

The *BNI5* ORF was introduced into the pH3C-LIC vector using the sequence- and ligation-independent cloning procedure. The *BNI5* ORF was inserted in frame with the N-terminal 8xHis tag followed by a 3C protease cleavage site. The pH3C-LIC vector contains a phage T7 promoter for driving transcription and a *lacO* element for regulation by IPTG. Site-directed mutagenesis reactions [66] with appropriate synthetic oligonucleotide primers were performed in series to introduce substitution mutations at pairs of the native Cys: Bni5 (C266F C375S), Bni5 (C144R C375S), and Bni5 (C144R C266F), designated Bni5 C144, Bni5 C266, and Bni5 C375, respectively. The substitutions chosen were derived in the following manner. In the Bni5 sequence from a commercial yeast (Foster's B), an Arg is found at the position corresponding to C144 in *S. cerevisiae* Bni5. Similarly, in the Bni5 sequence from the Foster's O strain, a Phe is found at the position corresponding to C266 in *S. cerevisiae* Bni5. Given its predicted solvent accessibility, we chose to replace the invariant C375 with Ser, a nearly isosteric and polar residue. In addition, we constructed both an N-terminal truncation, Bni5(Δ1–313) (which represents a 135-residue C-terminal fragment possessing only C375), and a C-terminal truncation, Bni5(C266F Δ314–448) (which represents a 313-residue N-terminal fragment possessing only C144).

Expression vector(s) was introduced into *Escherichia coli* strain NiCo21 (DE3; New England Biolabs), which has been engineered to remove the Ni^{2+}-binding ability of GlmS and several other endogenous *E. coli* proteins that commonly contaminate immobilized-metal ion affinity chromatography (IMAC) purifications (and some other typical *E. coli* protein contaminants are tagged with a chitin-binding domain permitting their removal by adsorption to chitin-agarose beads) [68,69]. Bacterial cultures were grown to an $A_{600\ nm}$ of 0.8–1.0, induced with IPTG (final concentration, 0.5 mM)

overnight at 16 °C, collected by centrifugation, and resuspended in ice-cold lysis buffer [300 mM KCl, 2 mM $MgCl_2$, 40 μM GDP, 0.1% monothioglycerol, 0.5% Tween 20, 12% glycerol, 20 mM imidazole, and 50 mM Tris–HCl (final pH 8.0) plus protease inhibitor mix (cOmplete EDTA-free; Roche) and 0.2 mg/mL lysozyme]. Cells were ruptured at 4 °C by six 15-s pulses of sonic irradiation using a Branson cell disrupter (model W185D) and separated by 15-s periods of cooling. The resulting lysate was clarified by centrifugation at 10,000*g* for 30 min at 4 °C. The clarified extract was subjected to IMAC on Ni^{2+}-nitrilotriacetate-agarose beads (Qiagen) in high-salt buffers [wash buffer: 300 mM KCl, 20 mM imidazole, and 50 mM Tris–HCl (final pH 8.0); elution buffer: 300 mM KCl, 500 mM imidazole, and 50 mM Tris–HCl (final pH 8.0)]. Fractions containing the bulk of the purified protein were combined, and the resulting pool (typically 5–6 mL) was passed over chitin-agarose beads (New England BioLabs) to remove three other endogenous *E. coli* gene products (ArnA, SlyD, and Can) that are the other known contaminants in IMAC-based purifications. The proteins in the flow-through from the chitin-agarose were loaded using the 10-mL loop of an AKTA FPLC system (GE Healthcare) onto a Superdex 200 HiLoad 16/60 column (16 mm × 60 cm; GE Healthcare) and were subjected to size-exclusion chromatography in septin buffer [300 mM KCl and 50 mM Tris–HCl (final pH 8.0)]. Fractions were collected, and the proteins present in each were resolved by SDS-PAGE and visualized by staining with Coomassie Blue dye. The peak fractions containing the highest concentrations of Bni5 or the stoichiometric concentration of septins were pooled and used immediately for labeling by maleimide chemistry.

Prior to reaction with maleimide dyes, the concentration of the purified protein products was determined by bicinchoninic acid (BCA) method (Pierce BCA protein assay kit; Life Technologies, Inc.) [70]. Samples were incubated with 10-fold molar excess of reducing agent tris-(2-carboxyethyl)phosphine for 10 min at room temperature, desalted by passage through Sephadex G25 (8.3 mL; PD-10 column; GE Healthcare) in labeling buffer [300 mM KCl and 50 mM Tris (final pH 7.0)] to remove the tris-(2-carboxyethyl)phosphine, and labeled overnight at 4 °C with a 5-fold molar excess of the desired maleimide dye (Alexa Fluor 488, AF555, and AF647; Life Technologies, Inc.). Excess dye was quenched with a 10-fold molar excess of DTT at room temperature for 10 min and removed by recapturing the 6xHis-Cdc12-containing septin complex or the 8xHis-tagged Bni5 by IMAC chromatography on a HisTrap HP column [GE Healthcare; wash buffer: 300 mM KCl, 20 mM imidazole, and 50 mM Tris–HCl (final pH 8.0); elution buffer: 300 mM KCl, 500 mM imidazole, and 50 mM Tris–HCl (final pH 8.0)]. The dye-labeled protein was dialyzed overnight against septin buffer [300 mM KCl and 50 mM Tris–HCl (final pH 8.0)] in a Slide-A-Lyzer dialysis cassette (Life Technologies, Inc.) with a 10-kDa molecular weight cutoff. The BCA assay (corrected for the contribution of the dye) and measurement of fluorescence using a P-330 Nanophotometer (Implen) were used to determine the molar concentration of protein and dye, respectively, in the final sample. In these complexes, in which only a single protomer type, for example, Cdc11, contained the sole Cys present, the efficiency of labeling was 0.7–0.8 dye molecules per Cys-containing subunit. Specificity of labeling was verified by resolving the subunits by SDS-PAGE and analyzing them by imaging with a Typhoon Trio Variable Mode Imager equipped for fluorescence (GE Healthcare) to detect the dye and by staining with Coomassie Blue dye and examining with an Odyssey scanner (Licor Biosciences) to detect the protein. Using the same criteria, the labeling efficiency for Bni5, which was mutated to contain only one Cys at one of three native locations, showed a similar average efficiency of labeling (0.7–0.8 dye molecules per protein molecule).

Fluorescence spectroscopy and data analysis

Emission spectra of 25-nM donor dye (AF555)-labeled septin hetero-octamers alone, serial dilutions of 500-nM acceptor dye (AF647)-labeled Bni5 proteins alone (unless otherwise specified), and mixtures of the two were measured in triplicate at room temperature after equilibration for 1 h in a cuvette (3-mm path length and 270-μL maximum volume) using a Cary Eclipse fluorescence spectrophotometer (Agilent). Unless specified otherwise, the final buffer conditions were 45 mM KCl and 50 mM Tris–HCl (pH 8.0). FRET values were obtained by subtracting the buffer-only background and correcting the emission spectrum of the acceptor for the contributions of both the donor and acceptor excited at 555 nm. Principal component analysis [71] and data fitting were done in Matlab (The Mathworks) and its toolboxes for curve fitting and statistics.

Analytical ultracentrifugation

Wild-type Bni5 (21.3 μM) was first exchanged into PBS buffer and concentrated using a centrifugal unit with a 10-kDa molecular weight cutoff. Buffer exchange was necessary for comparison with a reference cell during the experiment. All sedimentation experiments were performed at 50,000 rpm using a Beckman Coulter analytical ultracentrifuge equipped with a sole absorption optical scanner (Optima XLA). Partial specific volume for Bni5 (0.71852 mL/g), buffer density (1.00634 g/mL), and buffer viscosity (1.023 cP) were estimated using Sednterp [72]. Data were analyzed using Sedfit (using the Marquardt–Levenberg algorithm) and graphed using GUSSI [73].

FFF-MALS analysis

Wild-type Bni5, Bni5(1–313), Bni5(ΔHD), MBP-Bni5(314–448), and an MBP control were expressed and purified by methods described above. Each protein was exchanged into PBS and concentrated using a centrifugal concentrator with a 30-kDa molecular weight cutoff. Manipulations of the protein solutions were conducted with an autosampler (Agilent 1200 Series G1329A ALS) equipped with a pump for isocratic liquid flow (Agilent 1200 Series G1310A Isopump). Analysis of each protein solution was conducted using an FFF device (Wyatt Technology Eclipse 3) with a short channel and 10-kDa regenerated cellulose membrane, eluting with a decreasing 3 mL/min cross-flow ramp (the length of the ramp was varied to optimize the separation of any observed peaks). Species present were detected using MALS in a DAWN Heleos II (Wyatt Technology), and UV absorbance was measured with a multiple wavelength detector (Agilent 1100 Series G1365B), with in-line monitoring of refractive index using an OptiLab T-rEX (Wyatt Technology). Computational reduction of the output data obtained was performed using the Astra V software package (Wyatt Technology) and plotted as both light scattering and UV absorbance and, for each peak identified, accompanied by its calculated molar mass and the error (and, in parentheses, its percentage of the protein population).

Expression, purification, and labeling of septin complexes and Bni5 for EM analysis

Wild-type septin subunits were expressed from a single bicistronic DUET™ vector (EMD Millipore) as described previously [74]. Employing the In-FusionR HD Cloning Plus kit (Takara Clontech) and the *GFP* coding sequence, which was derived from pFastBac StrepII msfGFP TEV cloning vector with BioBrick PolyPromoter LIC Subcloning (438-Rgfp; Addgene plasmid #55,221), generously provided by Dr. Scott Gradia (QB3 MacroLab Core Facility, UC Berkeley), was fused to the C terminus of *CDC10* in the bicistronic DUET™ vector containing *CDC10* and the genes encoding the other three wild-type septin subunits. It has already been demonstrated that other Cdc10-GFP fusions do not adversely affect the functionality of Cdc10 [8,14]. Hetero-octamers capped with a CTE-less Cdc11 mutant, Cdc11(△357–415), were produced from two DUET™ vectors (EMD Millipore) as previously described [14,16]. The Bni5 construct employed is detailed in the FRET assay. No site-directed mutagenesis was performed on the vector; thus, 8xHis was fused to the N terminus of Bni5. The vectors for each septin octameric construct and Bni5 were each expressed as described above for the constructs employed in the FRET assay. Cells were harvested by centrifugation, resuspended in ice-cold lysis buffer, frozen, and stored at −80 °C until purification.

Frozen cell pellets for the septin complexes and Bni5 were thawed and agitated for 30 min in ice-cold water followed by sonication (Misonix 3000 sonicator) at 4 °C for six 30-s pulses separated by 2-min cooling intervals. The cell lysate was clarified by centrifugation at 25,000*g* for 45 min at 4 °C. The clarified lysate was incubated with chitin-agarose resin for 30 min to remove IMAC-contaminating proteins tagged with the chitin-binding domain [68,69]. The flow-through of septin complexes and other endogenous *E. coli* gene products was subjected to IMAC on Ni^{2+}-nitrilotriacetate-agarose beads (GE Healthcare) in high-salt buffers [wash buffer: 300 mM KCl, 25 mM imidazole, 50 mM Tris–HCl (pH 8.0 at 4 °C), and 0.1% monothioglycerol; elution buffer: 300 mM KCl, 300 mM imidazole, 50 mM Tris–HCl (pH 8.0 at 4 °C), and 0.1% monothioglycerol]. Fractions containing the highest concentration of protein [visually assessed by the Thermo Scientific™ Pierce™ Coomassie Plus™ (Bradford) Protein Assay and, separately, by A_{280nm} measurement *via* a NanoDrop 8000 (Thermo Scientific)] were combined and filtered with a 0.2-μm PDVF membrane. Then, 5 mL of the filtered product was loaded onto a Superdex 200 HiLoad 16/60 column (16 mm × 60 cm; GE Healthcare) *via* an AKTA FPLC system (GE Healthcare) for size-exclusion chromatography in septin buffer [300 mM KCl, 50 mM Tris–HCl (pH 8.0 at 4 °C), and 0.1% monothioglycerol]. Fractions collected with the highest concentration (A_{280nm} measurement with NanoDrop 8000) of stoichiometric septin subunit concentration (resolved by SDS-PAGE and visualized by Coomassie Blue dye) were pooled, aliquoted, flash frozen (liquid nitrogen), and stored at −80 °C until use.

For Bni5, fractions with the highest concentration were pooled and diluted to 150 mM KCl, 25 mM Tris–HCl (pH 8.0 at 4 °C), and 0.1% monothioglycerol. The diluted protein was loaded on a 1-mL HiTrap Q HP column (GE Healthcare) *via* the AKTA FPLC system (10-mL sample loop). Protein was eluted *via* a salt gradient from 150 mM KCl to 1 M KCl containing 25 mM Tris–HCl (pH 8.0 at 4 °C) and 0.1% monothioglycerol. Fractions were analyzed *via* SDS-PAGE and visualized by Coomassie Blue dye, and peak fractions were pooled and dialyzed overnight against septin buffer [300 mM KCl, 50 mM Tris–HCl (pH 8.0 at 4 °C), and 0.1% monothioglycerol] in a Slide-A-Lyzer dialysis cassette (Thermo Scientific) with a 10-kDa molecular weight cutoff. Final protein concentration was determined *via* A_{280nm} measurement with NanoDrop 8000, and aliquots were flash frozen (liquid nitrogen) and stored at −80 °C until use.

EM sample preparation, data collection, and analysis

All proteins were thawed on ice, and concentration was confirmed *via* A_{280nm} measurement with NanoDrop 8000. Septins (50 nM) alone and separately,

combined with Bni5 (250 nM), were incubated on ice for 5 min in low-salt conditions [45 mM KCl and 20 mM Tris–HCl (pH 8.0 at 4 °C)]. Then, 4 μL of the protein solution was placed on a continuous carbon grid [carbon supported by nitrocellulose on a copper grid (400 mesh)] that had been glow discharged (Solarus, Gatan). After the sample had adsorbed for about 1 min, half of the sample was blotted away, and the grid was rinsed in 40 μL of water and stained with 2% (wt/vol) uranyl formate (4 successive rinses of 40 μL each). Grids were blotted dry to remove excess solution. Samples were visualized, utilizing a Tecnai F20 transmission electron microscope (FEI) operating at 120 keV, and electron micrographs were collected at a magnification of 50,000× (2.29-Å pixel size) with an UltraScan 4000 CCD camera (Gatan). Data were collected, employing Leginon [75] implemented at a dose of 25 electrons per $Å^2$ and a defocus range from −0.75 to −0.95 μm. Approximately 500 micrographs were collected for each data set (Fig. S10).

Micrographs were processed within Appion [76]. The contrast transfer function of each micrograph was estimated using CTFFind v3 [77]. All distinguishable single pairs of septin filaments were selected manually by defining lines (helices) between the paired filaments (Fig. S10c). The lines were parsed into boxes (256 × 256 pixels) with 8-nm steps (approximate length of two septins subunits [14]), yielding approximately 65,000 particles per dataset. The resulting particle stacks were extracted from images, in which Ace2 [78] was employed to flip the phase, and subsequently normalized using XMIPP [79] to remove pixels beyond a 4.5σ of the mean value.To reduce the computation time required for processing, each image in the particle stack was binned by two, and 2D alignment and classification were performed with iterative multi-variate statistical analysis/multireference alignment (MSA/MRA) [80]. A mask was applied such that full-size septin octamer (32 nm) would be flanked on either side by approximately three additional septin subunits, and typically, 8 iterations were performed to yield approximately 250 classes (Fig. S10d). 2D class averages were subjected to a custom SPIDER script [81] to determine the radon transform (Fig. S10e) of each class and extract the maximum peak intensities with their corresponding angles and distance from the image midpoint. Python (version 2.7) was employed to tally the angle difference between the two maximum peaks in individual radon transforms. For angle differences less than 20 degrees, the distance between the peaks was determined, thus giving the distance between the septin filaments in the individual class averages. Final distance values were aggregated into histograms, normalized, and fit with appropriate probability density functions using Matlab. A single normal distribution was fit to the data for septins alone, and a weighted sum of two normal distributions was fit to the data for septins with Bni5 [$M = \alpha N(\mu_1\sigma_1^2) + (1\text{-}\alpha)N(\mu_2\sigma_2^2)$]. The weight of the two normal distribution mixture is called the mixture weight (α), which determines the contribution of each distribution to the mixture probability density function (M). EMAN was employed to determine the aligned difference map between 2D class averages [82].

Acknowledgments

This work was supported by National Institutes of Health R01 Grants GM21841 (to J.T.) and GM101314 (to J.T. and E.N.). E.N. is an Investigator of the Howard Hughes Medical Institute (HHMI). We thank members of the Thorner and Nogales Labs for helpful comments and suggestions during the course of these studies. We especially thank John Hall at Grifols Diagnostics Solutions, Inc. for sharing his expertise with FFF-MALS and for technical assistance with our FFF-MALS experiments.

Author contributions: E.A.B. conducted FRET, FFF-MALS, and fluorescence microscopy experiments and analyzed the data. S.M.S. conducted EM experiments and analyzed the data. D.D. conducted the analytical ultracentrifugation and analyzed the data. E.N. and J.T. also analyzed the data. E.A.B., S.M.S., E.N., and J.T. designed the experiments and wrote the manuscript.

Conflict of interest statement: The authors declare that they have no conflicts of interest that have affected or influenced the contents of this article.

Appendix A. Supplementary Data

Supplementary data to this article can be found online at doi:10.1016/j.jmb.2016.10.024.

Received 10 June 2016;
Received in revised form 17 October 2016;
Accepted 24 October 2016
Available online 30 October 2016

Keywords:
yeast (*Saccharomyces cerevisiae*);
FRET analysis;
electron microscopy;
analytical ultracentrifugation;
field-flow fractionation

Present address: E.A. Booth, Department of Research and Development, Grifols Diagnostic Solutions, Inc., 4560 Horton St., Emeryville, CA 94608, USA.

Present address: D. Dovala, Novartis Institute for BioMedical Research, 5300 Chiron Way, Emeryville, CA 94608, USA.

†E.A.B. and S.M.S. contributed equally to this work.

Abbreviations used:
AF555, Alexa Fluor 555; AF647, Alexa Fluor 647; BCA, bicinchoninic acid; *cdc*, cell division cycle; CTE, C-terminal extension; EM, electron microscopy; FFF, field-flow fractionation; FFF-MALS, FFF analyzed by multi-angle light scattering; FRET, Förster resonance energy transfer; MALS, multi-angle light scattering; ts, temperature-sensitive.

References

[1] F. Pan, R.L. Malmberg, M. Momany, Analysis of septins across kingdoms reveals orthology and new motifs, BMC Evol. Biol. 7 (2007) 103.

[2] R. Nishihama, M. Onishi, J.R. Pringle, New insights into the phylogenetic distribution and evolutionary origins of the septins, Biol. Chem. 392 (2011) 681–687.

[3] L.H. Hartwell, Genetic control of the cell division cycle in yeast. IV. Genes controlling bud emergence and cytokinesis, Exp. Cell Res. 69 (1971) 265–276.

[4] L.H. Hartwell, J. Culotti, J.R. Pringle, B.J. Reid, Genetic control of the cell division cycle in yeast, Science 183 (1974) 46–51.

[5] C.W. Carroll, R. Altman, D. Schieltz, J.R. Yates, D. Kellogg, The septins are required for the mitosis-specific activation of the Gin4 kinase, J. Cell Biol. 143 (1998) 709–717.

[6] A. Mino, K. Tanaka, T. Kamei, M. Umikawa, T. Fujiwara, Y. Takai, Shs1p: a novel member of septin that interacts with spa2p, involved in polarized growth in *Saccharomyces cerevisiae*, Biochem. Biophys. Res. Commun. 251 (1998) 732–736.

[7] B.K. Haarer, J.R. Pringle, Immunofluorescence localization of the *Saccharomyces cerevisiae CDC12* gene product to the vicinity of the 10-nm filaments in the mother-bud neck, Mol. Cell. Biol. 7 (1987) 3678–3687.

[8] V.J. Cid, L. Adamíková, R. Cenamor, M. Molina, M. Sánchez, C. Nombela, Cell integrity and morphogenesis in a budding yeast septin mutant, Microbiology 144 (1998) 3463–3474.

[9] B. Byers, L. Goetsch, Highly ordered ring of membrane-associated filaments in budding yeast, J. Cell Biol. 69 (1976) 717–721.

[10] G. Garcia, A. Bertin, Z. Li, Y. Song, M.A. McMurray, J. Thorner, E. Nogales, Subunit-dependent modulation of septin assembly: budding yeast septin Shs1 promotes ring and gauze formation, J. Cell Biol. 195 (2011) 993–1004.

[11] M. Versele, J. Thorner, Septin collar formation in budding yeast requires GTP binding and direct phosphorylation by the PAK Cla4, J. Cell Biol. 164 (2004) 701–715.

[12] M. Farkasovsky, P. Herter, B. Voss, A. Wittinghofer, Nucleotide binding and filament assembly of recombinant yeast septin complexes, Biol. Chem. 386 (2005) 643–656.

[13] M. Versele, M.J. Shulewitz, V.J. Cid, S. Bahmanyar, R.E. Chen, P. Barth, T. Alber, J. Thorner, Protein–protein interactions governing septin heteropentamer assembly and septin filament organization in *Saccharomyces cerevisiae*, Mol. Biol. Cell 15 (2004) 4568–4583.

[14] A. Bertin, M.A. Mcmurray, P. Grob, S.-S. Park, G. Garcia, I. Patanwala, H.L. Ng, T. Alber, J. Thorner, E. Nogales, *Saccharomyces cerevisiae* septins: supramolecular organization of heterooligomers and the mechanism of filament assembly, Proc. Natl. Acad. Sci. U. S. A. 105 (2008) 8274–8279.

[15] C. Renz, N. Johnsson, T. Gronemeyer, An efficient protocol for the purification and labeling of entire yeast septin rods from *E. coli* for quantitative *in vitro* experimentation, BMC Biotechnol. 13 (2013) 60.

[16] E.A. Booth, E.W. Vane, D. Dovala, J. Thorner, A Förster resonance energy transfer (FRET)-based system provides insight into the ordered assembly of yeast septin hetero-octamers, J. Biol. Chem. 290 (2015) 28,388–28,401.

[17] C. Kaplan, B. Jing, C.M. Winterflood, A.A. Bridges, P. Occhipinti, J. Schmied, S. Grinhagens, T. Gronemeyer, P. Tinnefeld, A.S. Gladfelter, J. Ries, H. Ewers, The absolute arrangement of subunits in cytoskeletal septin filaments in cells measured by fluorescence microscopy, Nano Lett. 15 (2015) 3859–3864.

[18] A. Bertin, M.M. Ma, L. Thai, G. Garcia, V. Votin, P. Grob, T. Allyn, J. Thorner, E. Nogales, Phosphatidylinositol-4,5-bisphosphate promotes budding yeast septin filament assembly and organization, J. Mol. Biol. 404 (2010) 711–731.

[19] A.A. Bridges, H. Zhang, S.B. Mehta, P. Occhipinti, T. Tani, A.S. Gladfelter, Septin assemblies form by diffusion-driven annealing on membranes, Proc. Natl. Acad. Sci. U. S. A. 111 (2014) 2146–2151.

[20] G.C. Finnigan, J. Takagi, C. Cho, J. Thorner, Comprehensive genetic analysis of paralogous terminal septin subunits Shs1 and Cdc11 in *Saccharomyces cerevisiae*, Genetics 200 (2015) 841–861.

[21] M.S. Kim, C.D. Froese, M.P. Estey, W.S. Trimble, SEPT9 occupies the terminal positions in septin octamers and mediates polymerization-dependent functions in abscission, J. Cell Biol. 195 (2011) 815–826.

[22] M.E. Sellin, L. Sandblad, S. Stenmark, M. Gullberg, Deciphering the rules governing assembly order of mammalian septin complexes, Mol. Biol. Cell 22 (2011) 3152–3164.

[23] M. Sirajuddin, M. Farkasovsky, F. Hauer, D. Kühlmann, I.G. Macara, M. Weyand, H. Stark, A. Wittinghofer, Structural insight into filament formation by mammalian septins, Nature 449 (2007) 311–315.

[24] E. Zent, I. Vetter, A. Wittinghofer, Structural and biochemical properties of Sept7, a unique septin required for filament formation, Biol. Chem. 392 (2011) 791–797.

[25] J.N. Macedo, N.F. Valadares, I.A. Marques, F.M. Ferreira, J.C.P. Damalio, H.M. Pereira, R.C. Garratt, A.P. Araujo, The structure and properties of septin 3: a possible missing link in septin filament formation, Biochem. J. 450 (2013) 95–105.

[26] M. Sirajuddin, M. Farkasovsky, E. Zent, A. Wittinghofer, GTP-induced conformational changes in septins and implications for function, Proc. Natl. Acad. Sci. U. S. A. 106 (2009) 16,592–16,597.

[27] A.E. Zeraik, H.M. Pereira, Y.V. Santos, J. Brandão-Neto, M. Spoerner, M.S. Santos, L.A. Colnago, R.C. Garratt, A.P. Araújo, R. DeMarco, Crystal structure of a *Schistosoma mansoni* septin reveals the phenomenon of strand slippage in septins dependent on the nature of the bound nucleotide, J. Biol. Chem. 289 (2014) 7799–7811.

[28] A. Brausemann, S. Gerhardt, S. A-k, O. Einsle, A. Große-berkenbusch, N. Johnsson, T. Gronemeyer, Crystal structure of Cdc11, a septin subunit from *Saccharomyces cerevisiae*, J. Struct. Biol. 193 (2016) 157–161.

[29] E. Zent, A. Wittinghofer, Human septin isoforms and the GDP-GTP cycle, Biol. Chem. 395 (2014) 169–180.

[30] G.C. Finnigan, E.A. Booth, A. Duvalyan, E.N. Liao, J. Thorner, The carboxy-terminal tails of septins Cdc11 and

Shs1 recruit myosin-II binding factor Bni5 to the bud neck in *Saccharomyces cerevisiae*, Genetics 200 (2015) 843–862.
[31] P.A. Takizawa, J.L. DeRisi, J.E. Wilhelm, R.D. Vale, Plasma membrane compartmentalization in yeast by messenger RNA transport and a septin diffusion barrier, Science 290 (2000) 341–344.
[32] F. Caudron, Y. Barral, Septins and the lateral compartmentalization of eukaryotic membranes, Dev. Cell 16 (2009) 493–506.
[33] Y. Tanaka-Takiguchi, M. Kinoshita, K. Takiguchi, Septin-mediated uniform bracing of phospholipid membranes, Curr. Biol. 19 (2009) 140–145.
[34] M. Mavrakis, Y. Azou-Gros, F. Tsai, J. Alvarado, A. Bertin, F. Iv, A. Kress, S. Brasselet, G.H. Koenderink, T. Lecuit, Septins promote F-actin ring formation by crosslinking actin filaments into curved bundles, Nat. Cell Biol. 16 (2014) 322–334.
[35] A.A. Bridges, A.S. Gladfelter, Septin form and function at the cell cortex, J. Biol. Chem. 290 (2015) 17,173–17,180.
[36] A.S. Gladfelter, J.R. Pringle, D.J. Lew, The septin cortex at the yeast mother-bud neck, Curr. Opin. Microbiol. 4 (2001) 681–689.
[37] M.A. McMurray, J. Thorner, Septins: molecular partitioning and the generation of cellular asymmetry, Cell Div. 4 (2009) 18.
[38] Y. Oh, E. Bi, Septin structure and function in yeast and beyond, Trends Cell Biol. 21 (2011) 141–148.
[39] J.P. Caviston, M. Longtine, J.R. Pringle, E. Bi, The role of Cdc42p GTPase-activating proteins in assembly of the septin ring in yeast, Mol. Biol. Cell 14 (2003) 4051–4066.
[40] J. Dobbelaere, M.S. Gentry, R.L. Hallberg, Y. Barral, Phosphorylation-dependent regulation of septin dynamics during the cell cycle, Dev. Cell 4 (2003) 345–357.
[41] K. Ong, C. Wloka, S. Okada, T. Svitkina, E. Bi, Architecture and dynamic remodelling of the septin cytoskeleton during the cell cycle, Nat. Commun. 81 (2014) 8715–8723.
[42] P.R. Lee, S. Song, H.S. Ro, C.J. Park, J. Lippincott, R. Li, J.R. Pringle, C. De Virgilio, M.S. Longtine, K.S. Lee, Bni5p, a septin-interacting protein, is required for normal septin function and cytokinesis in *Saccharomyces cerevisiae*, Mol. Cell. Biol. 22 (2002) 6906–6920.
[43] S.C. Nam, H. Sung, S.H. Kang, J.Y. Joo, S.J. Lee, Y.B. Chung, C.K. Lee, S. Song, Phosphorylation-dependent septin interaction of Bni5 is important for cytokinesis, J. Microbiol. (Seoul Korea) 45 (2007) 227–233.
[44] S.C. Nam, H. Sung, Y.B. Chung, C.-K. Lee, D.H. Lee, S. Song, Requirement of Bni5 phosphorylation for bud morphogenesis in *Saccharomyces cerevisiae*, J. Microbiol. (Seoul Korea) 45 (2007) 34–40.
[45] X. Fang, J. Luo, R. Nishihama, C. Wloka, C. Dravis, M. Travaglia, M. Iwase, E.A. Vallen, E. Bi, Biphasic targeting and cleavage furrow ingression directed by the tail of a myosin II, J. Cell Biol. 191 (2010) 1333–1350.
[46] C. Schneider, J. Grois, C. Renz, T. Gronemeyer, N. Johnsson, Septin rings act as template for myosin higher-order structures and inhibit redundant polarity establishment, J. Cell Sci. 126 (2013) 3390–3400.
[47] C. Patasi, J. Godočíková, S. Michlíková, Y. Nie, R. Káčeriková, K. Kválová, S. Raunser, M. Farkašovský, The role of Bni5 in the regulation of septin higher-order structure formation, Biol. Chem. 396 (2015) 1325–1337.
[48] E.A. Booth, J. Thorner, A FRET-based method for monitoring septin polymerization and binding of septin-associated proteins, Methods Cell Biol. 136 (2016) 35–56.
[49] M.A. McMurray, A. Bertin, G. Garcia 3rd, L. Lam, E. Nogales, J. Thorner, Septin filament formation is essential in budding yeast, Dev. Cell 20 (2011) 540–549.
[50] L.A. Kelley, S. Mezulis, C.M. Yates, M.N. Wass, M.J.E. Sternberg, The Phyre2 web portal for protein modeling, prediction and analysis, Nat. Protoc. 10 (2015) 845–858.
[51] Y.M. Soh, F. Bürmann, H.C. Shin, T. Oda, K.S. Jin, C.P. Toseland, C. Kim, H. Lee, S.J. Kim, M.S. Kong, M.L. Durand-Diebold, Y.G. Kim, H.M. Kim, N.K. Lee, M. Sato, B.H. Oh, S. Gruber, Molecular basis for SMC rod formation and its dissolution upon DNA binding, Mol. Cell 57 (2015) 290–303.
[52] T. Gligoris, J. Löwe, Structural insights into ring formation of cohesin and related SMC complexes, Trends Cell Biol. 26 (2016) 680–693.
[53] N. de Val, M.A. McMurray, L.H. Lam, C.C. Hsiung, A. Bertin, E. Nogales, J. Thorner, Native cysteine residues are dispensable for the structure and function of all five yeast mitotic septins, Proteins 81 (2013) 1964–1979.
[54] F. Sievers, D.G. Higgins, Clustal Omega, accurate alignment of very large numbers of sequences, Methods Mol. Biol. 1079 (2014) 105–116.
[55] P.J. Britto, L. Knipling, J. Wolff, The local electrostatic environment determines cysteine reactivity of tubulin, J. Biol. Chem. 277 (2002) 29,018–29,027.
[56] P.C. Lyu, J.C. Sherman, A. Chen, N.R. Kallenbach, Alpha-helix stabilization by natural and unnatural amino acids with alkyl side chains, Proc. Natl. Acad. Sci. U. S. A. 88 (1991) 5317–5320.
[57] A.A. Rodal, L. Kozubowski, B.L. Goode, D.G. Drubin, J.H. Hartwig, Actin and septin ultrastructures at the budding yeast cell cortex, Mol. Biol. Cell 16 (2005) 372–384.
[58] A. Bertin, M.M. Ma, J. Pierson, L. Thai, K.L. McDonald, E.A. Zehr, G. García III, P. Peters, J. Thorner, E. Nogales, Three-dimensional ultrastructure of the septin filament network in *Saccharomyces cerevisiae*, Mol. Biol. Cell 23 (2012) 423–432.
[59] T.R. Patel, D.J. Winzor, D.J. Scott, Analytical ultracentrifugation: a versatile tool for the characterisation of macromolecular complexes in solution, Methods 95 (2016) 55–61.
[60] J.C. Giddings, Field-flow fractionation: analysis of macromolecular, colloidal, and particulate materials, Science 260 (1993) 1456–1465.
[61] S. Schachermeyer, J. Ashby, W. Zhong, Advances in field-flow fractionation for the analysis of biomolecules: instrument design and hyphenation, Anal. Bioanal. Chem. 404 (2012) 1151–1158.
[62] A. Casamayor, M. Snyder, Molecular dissection of a yeast septin: distinct domains are required for septin interaction, localization, and function, Mol. Cell. Biol. 23 (2003) 2762–2777.
[63] J.P. Schneider, A. Lombardi, W.F. DeGrado, Analysis and design of three-stranded coiled coils and three-helix bundles, Fold. Des. 3 (1998) R29–R40.
[64] Y. Sadian, C. Gatsogiannis, C. Patasi, O. Hofnagel, R.S. Goody, M. Farkasovský, S. Raunser, The role of Cdc42 and Gic1 in the regulation of septin filament formation and dissociation, Elife 2 (2013) e01085.
[65] M. Iwase, J. Luo, S. Nagaraj, M. Longtine, H.B. Kim, B.K. Haarer, C. Caruso, Z. Tong, J.R. Pringle, E. Bi, Role of a Cdc42p effector pathway in recruitment of the yeast septins to the presumptive bud site, Mol. Biol. Cell 17 (2006) 1110–1125.
[66] W. Wang, B.A. Malcolm, Two-stage PCR protocol allowing introduction of multiple mutations, deletions and insertions using QuikChange™ site-directed mutagenesis, BioTechniques 26 (1999) 680–682.
[67] M.Z. Li, S.J. Elledge, Harnessing homologous recombination *in vitro* to generate recombinant DNA *via* SLIC, Nat. Methods 4 (2007) 251–256.
[68] V.M. Bolanos-Garcia, O.R. Davies, Structural analysis and classification of native proteins from *E. coli* commonly co-

purified by immobilised metal affinity chromatography, Biochim. Biophys. Acta 1760 (2006) 1304–1313.
[69] C. Robichon, J. Luo, T.B. Causey, J.S. Benner, J.C. Samuelson, Engineering *Escherichia coli* BL21(DE3) derivative strains to minimize *E. coli* protein contamination after purification by immobilized metal affinity chromatography, Appl. Environ. Microbiol. 77 (2011) 4634–4646.
[70] P.K. Smith, R.I. Krohn, G.T. Hermanson, A.K. Mallia, F.H. Gartner, M.D. Provenzano, E.K. Fujimoto, N.M. Goeke, B.J. Olson, D.C. Klenk, Measurement of protein using bicinchoninic acid, Anal. Biochem. 150 (1985) 76–85.
[71] Al-Soufi W, Novo M, Mosquera M, Rodríguez-Prieto F (2009) Principal component global analysis of series of fluorescence spectra, In Reviews in Fluorescence (Geddes CD, ed.) pp. 23–45, Springer-Verlag, Inc., New York, NY.
[72] Laue TM, Shah BD, Ridgeway TM, Pelletier SL (1992) Computer-aided interpretation of analytical sedimentation data for proteins, In Analytical Ultracentrifugation in Biochemistry and Polymer Science (Harding, SE, Rowe AJ, Horton JC, eds.), pp. 90–125, Royal Society of Chemistry, London, UK.
[73] P. Schuck, Size-distribution analysis of macromolecules by sedimentation velocity ultracentrifugation and lamm equation modeling, Biophys. J. 78 (2000) 1606–1619.
[74] G.C. Finnigan, S.M. Sterling, A. Duvalyan, E.N. Liao, A. Sargsyan, G. Garcia 3rd, E. Nogales, J. Thorner, Coordinate action of distinct sequence elements localizes checkpoint kinase Hsl1 to the septin collar at the bud neck in *Saccharomyces cerevisiae*, Mol. Biol. Cell 27 (2016) 2213–2233.
[75] C. Suloway, J. Pulokas, D. Fellmann, A. Cheng, F. Guerra, J. Quispe, S. Stagg, C.S. Potter, B. Carragher, Automated molecular microscopy: the new Leginon system, J. Struct. Biol. 151 (2005) 41–60.
[76] G.C. Lander, S.M. Stagg, N.R. Voss, A. Cheng, D. Fellmann, J. Pulokas, C. Yoshioka, C. Irving, A. Mulder, P.W. Lau, D. Lyumkis, C.S. Potter, B. Carragher, Appion: an integrated, database-driven pipeline to facilitate EM image processing, J. Struct. Biol. 166 (2009) 95–102.
[77] J.A. Mindell, N. Grigorieff, Accurate determination of local defocus and specimen tilt in electron microscopy, J. Struct. Biol. 142 (2003) 334–347.
[78] S.P. Mallick, B. Carragher, C.S. Potter, D.J. Kriegman, ACE: automated CTF estimation, Ultramicroscopy 104 (2005) 8–29.
[79] R. Marabini, I.M. Masegosa, M.C. San Martin, S. Marco, J.J. Fernandez, L.G. de la Fraga, C. Vaquerizo, J.M. Carazo, Xmipp: an image processing package for electron microscopy, J. Struct. Biol. 116 (1996) 237–240.
[80] T. Ogura, K. Iwasaki, C. Sato, Topology representing network enables highly accurate classification of protein images taken by cryo electron-microscope without masking, J. Struct. Biol. 143 (2003) 185–200.
[81] J. Frank, M. Radermacher, P. Penczek, J. Zhu, Y. Li, M. Ladjadj, A. Leith, SPIDER and WEB: processing and visualization of images in 3D electron microscopy and related fields, J. Struct. Biol. 116 (1996) 190–199.
[82] S.J. Ludtke, P.R. Baldwin, W. Chiu, EMAN: semiautomated software for high-resolution single-particle reconstructions, J. Struct. Biol. 128 (1999) 82–97.
[83] G.E. Crooks, G. Hon, J.M. Chandonia, S.E. Brenner, WebLogo: a sequence logo generator, Genome Res. 14 (2004) 1188–1190.